Application of calorimetry to the assessment of the performance of ITER Nb_3Sn TF conductor samples in SULTAN tests

2008 Supercond. Sci. Technol. 21 105004

(http://iopscience.iop.org/0953-2048/21/10/105004)

Supercond. Sci. Technol. **21** (2008) 105004 (12pp) doi:10.1088/0953-2048/21/10/105004

Application of calorimetry to the assessment of the performance of ITER Nb_3Sn TF conductor samples in SULTAN tests

L Savoldi Richard and R Zanino

Dipartimento di Energetica, Politecnico, I-10129 Torino, Italy

E-mail: roberto.zanino@polito.it

Received 5 February 2008, in final form 15 June 2008
Published 23 July 2008
Online at stacks.iop.org/SUST/21/105004

Abstract

In the frame of the International Thermonuclear Experimental Reactor (ITER), several short full-size Nb_3Sn samples of candidate toroidal field (TF) conductors were tested in 2007 at the SULTAN facility, PSI Villigen, Switzerland, in conditions relevant to the ITER TF (background magnetic field of 10.78 T and transport current of 68 kA). The performance of a SULTAN sample is determined by the current sharing temperature T_{CS}. This can be obtained in principle from voltage measurements along the conductor sample, but the procedure is not free of issues and ambiguities. Here a complementary approach, based on the calorimetric assessment of the Joule heating due to current sharing, is critically discussed. Suitable algorithms are defined and the respective error bars are estimated, also based on numerical thermal–hydraulic modeling. The calorimetric approach is then applied to assess the performance of the samples tested in 2007 and compared with the results of the standard (electrical) approach.

(Some figures in this article are in colour only in the electronic version)

1. Introduction

Toroidal field (TF) conductor samples have been tested in the SULTAN facility (Villigen, Switzerland) for the last 10 years or so within the framework of the ITER R&D program. In particular, Nb_3Sn conductor samples of the ITER TF model coil were tested as early as 1999 (Ciazynski *et al* 2000); after testing the model coil (Savoldi *et al* 2002, Zanino and Richard 2003, Heller *et al* 2003, Ulbricht *et al* 2005) an attempt to compare the performance of short samples and model coils was also made (Zanino *et al* 2005).

In view of the performance degradation observed during these tests, compared with single strand measurements (Taylor and Hampshire 2005), a new R&D effort was launched using advanced (higher performance) strands in the similar conductor layout (Bruzzone *et al* 2008a), but this did not give the expected improvement in conductor performance (Ciazynski 2007). Since strand bending and pinching had meanwhile been identified as critical issues (Mitchell 2005, Nijhuis *et al* 2005), an improved conductor layout based on a lower void fraction and/or longer cabling twist pitches (see figure 1) was proposed (Nijhuis and Ilyin 2006) as a means of increasing the support for the strands thereby reducing the bending and the contact pressure.

During 2007 several short samples of ITER TF conductors were tested in SULTAN (Bruzzone *et al* 2008a, 2008b). The detailed geometrical and material data for all conductors discussed in this paper can be found in Bruzzone *et al* (2008b) and will not be repeated here. The main purpose of these tests, included in the so-called R&D 'crash program', was to see if the new cable layout could indeed improve conductor performance with respect to previously tested samples. Reference ITER-relevant conditions for the performance assessment were transport current $I_{sample} = I^{ref}_{sample} = 68$ kA and external field $B_{SULTAN} = B^{ref}_{SULTAN} = 10.78$ T. Typically, the current was ramped up to I^{ref}_{sample} at B^{ref}_{SULTAN}, inlet temperature $T_{in} = 4.5$ K, pressure ~10 MPa and mass flow rate from 2 to 4 g s^{-1}; then T_{in} was increased until quenching.

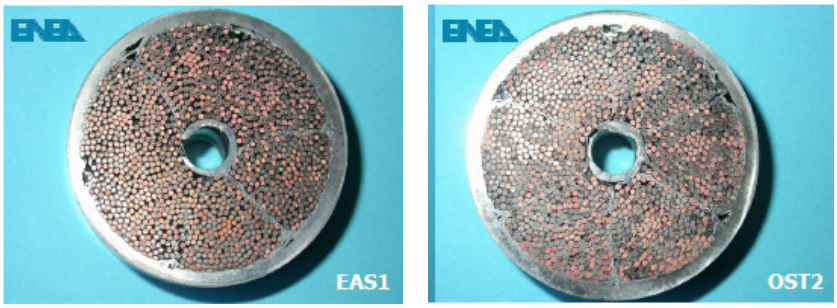

Figure 1. Left: cross section of the TFPRO1 left leg with the ITER TF reference void fraction (∼34%). Right: cross section of the TFPRO2 left leg with reduced void fraction (∼28%). In both conductors the six last-but-one wrapped cabling stages ('petals') are clearly visible; the open 'triangles' between two adjacent petal wrappings and the jacket can also be seen.

Table 1. Major calorimetric features of ITER TF short sample SULTAN tests in 2007.

Sample	Baseline run	Heating	Central channel	Additional temp. sensors
TFPRO1	No	Transient	Plugged	No
TFPRO2 (first test)	Transient	Transient	Plugged	No
TFPRO2 (re-test)	Quasi-steady	Quasi-steady	Plugged	Yes (extended diagnostics)
KOTF	Quasi-steady	Quasi-steady	Plugged	Yes (T7, T8)
JATF1	Quasi-steady	Quasi-steady	Free	No
JATF2 (first test)	Quasi-steady	Quasi-steady	Plugged	No
JATF2 (re-test)	Quasi-steady	Quasi-steady	Plugged	Yes (extended diagnostics)
RFTF1	Quasi-steady	Quasi-steady	Plugged	Yes (T7, T8)

In view of the difficulties in the interpretation of voltage signals that often present a non-zero offset at the end of the current ramp (Bruzzone *et al* 2008a), as already noted in previous sample tests (Bruzzone *et al* 2007), a complementary calorimetric approach was proposed for the assessment of T_{CS} (Bruzzone *et al* 2008b, Bessette and Mitchell 2008). This approach relies in principle on accurate and sufficiently detailed thermometry, as well as on steady-state operation—not always verified in practice (see table 1) although improved from test to test.

The two key measurements for calorimetry are obviously those of temperature and of mass flow rate. The mass flow rate is measured separately on each leg at the conductor outlet. The reference thermometer set-up, adopted for all samples tested in 2007 up to August, is shown in figure 2(a). Except for the inlet thermometers T1 and T2, all other thermometers were mounted on the conductor jacket. Since testing of all samples except JATF1 (Bessette and Mitchell 2008) was carried out with the central channel plugged in the high-field region, i.e. up to 1.5 m from the joint inlet (Bruzzone *et al* 2008b), this temperature should be to some extent representative of the temperature in the annular region occupied by the strands, in view also of the long timescales (quasi-steady-state) involved in most of these transients. In a couple of samples, additional thermometers (T7, T8) were mounted on the same cross section but opposite T5, T6, respectively. A re-test of the TFPRO2 and JATF2 samples was also performed, with the sample equipped with extended diagnostics (see figure 2(b)).

While scattered results of calorimetric analyses of single samples have been presented recently (Bruzzone *et al* 2008b, Kim *et al* 2008, Takahashi *et al* 2008) this paper represents, to the best of our knowledge, the first systematic attempt at a calorimetric analysis of the whole set of ITER TF samples tested in SULTAN during 2007.

2. The use of calorimetry for T_{CS} assessment

The calorimetric estimate of the voltage across a reference length of conductor (control volume, CV) in the high-field region is given by

$$V_{cal} = \Phi / I_{sample} \tag{1}$$

where Φ is the Joule power generated inside the CV. When evaluating T_{CS} by calorimetry, Φ has to be computed from measured temperatures, pressures and mass flow rates.

In SULTAN, the voltage threshold to be retained for the calorimetric definition of T_{CS} is slightly higher than that used for the electrical one, since the distance $\Delta L_T = 500$ mm between the high-field thermometers (e.g. T3 and T5) is larger than the distance $\Delta L_V = 450$ mm between the reference voltage taps (e.g. V3 and V9)[1]. For an average electric field between the taps equal to the critical value $E_C = 10\ \mu V\ m^{-1}$, the voltage threshold for the electrical measurement ($=E_C \times \Delta L_V$) is 4.5 μV. The Mithrandir code (Zanino *et al* 1995) was used to simulate a T_{CS} measurement using for the cable n-index the ITER reference value of 7 (ITER 2004). A voltage $V^{thres} = 4.8\ \mu V$ between the high-field thermometers was computed corresponding to the 4.5 μV between voltage taps. The non-negligible difference between the two voltages is due to the

[1] Another pair of voltage taps was present in the standard instrumentation but not shown in figure 2; they are also located across the high-field region, albeit only 350 mm apart (i.e. at a distance significantly shorter than the petal twist pitch).

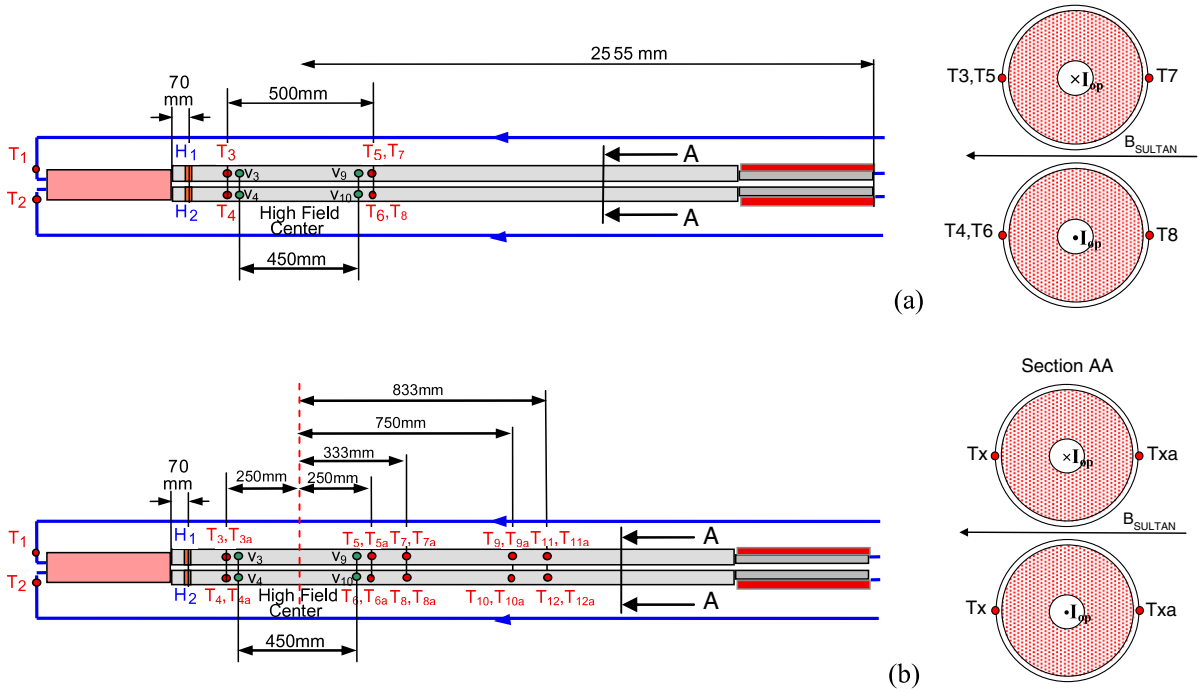

Figure 2. SULTAN sample thermometry and reference voltage taps: (a) standard set-up, (b) enhanced diagnostics. The distribution of thermometers along the conductors/legs is shown in the left part of the figure, together with the He flow direction. The location of the thermometer on the conductor cross section is shown in the right part of the figure, together with transport current and external (SULTAN) magnetic field direction. Odd sensor numbers correspond to the left leg, even numbers to the right leg.

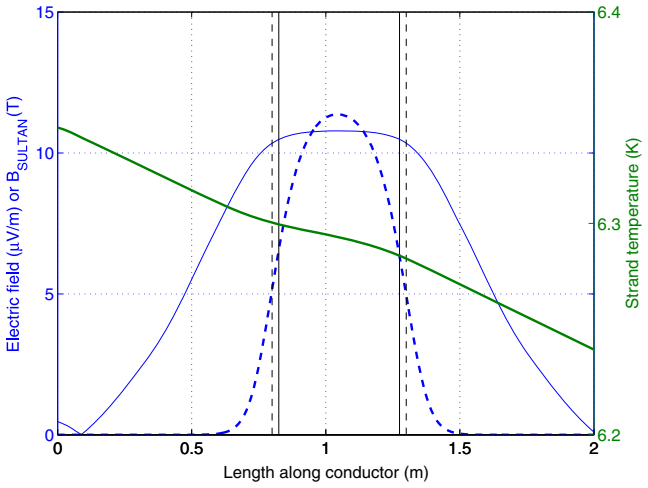

Figure 3. Spatial profile of the background magnetic field BSULTAN (thin solid line) and electric field (dashed line) computed along the conductor (left axis), and spatial profile of the computed strand temperature, for an average electric field of 10 μV m^{-1} between the voltage taps (right axis), in the case of transient inlet heating. The vertical solid and dashed lines indicate the position of the high-field voltage taps and thermometers, respectively. The zero abscissa is located at the joint inlet.

profile of the background magnetic field along the conductor axis (see figure 3), still significantly high in the restricted space between voltage and temperature taps. Note that, due to the non-uniform profile of the electric field (see figure 3) V^{thres} does not simply increase proportionally to the increased distance between the taps.

V_{cal} might not fully correspond to the average measured voltage (even if the taps were at the thermometer locations) in the case of an uneven current distribution among the strands (and in particular among the petals) and current transfer within the CV. We assume here uniform current distribution in the sample, according to the results reported in Cau *et al* (2008). The impact of current non-uniformity on the performance of SULTAN samples, including the effect of the jacket on the interpretation of the voltage signals (Breschi and Ribani 2007), is currently under investigation using the THELMA code (Bellina *et al* 2008, Breschi *et al* 2008).

In order to estimate Φ to be used in (1), we apply the (transient) energy balance (first principle of thermodynamics) to the portion of cable-in-conduit conductor (CICC) between the temperature sensors upstream and downstream of the high-field region, which defines the relevant CV:

$$\left(\frac{\mathrm{d}U}{\mathrm{d}t}\right)_{\text{CV}} = \Phi - W_{\text{cond}} - \left(\frac{\mathrm{d}m}{\mathrm{d}t}\right)_{\text{out}} h_{\text{out}} + \left(\frac{\mathrm{d}m}{\mathrm{d}t}\right)_{\text{in}} h_{\text{in}} \quad (2)$$

where U is the total internal energy inside the CV, W_{cond} is total power loss by heat conduction from the CV (mainly along the Cu in the strands—note the typically transient temperature profile in figure 3, the result of Joule heating superposed to transient inlet helium heating), $\mathrm{d}m/\mathrm{d}t$ is the mass flow rate, which is assumed to be characterized by the average specific enthalpy h (on the inflow and outflow cross sections, respectively), which is a function of the local average pressure[2] and temperature.

[2] For the sake of simplicity, the specific enthalpy may be computed everywhere using the measured inlet pressure ∼1 MPa, the dependence of enthalpy on pressure being very weak in the test conditions.

The main assumption behind (2) is that the CICC surface is adiabatic. For the limited purpose of improving the accuracy of the assessment of T_{CS}, the heat loss W_{cond} was computed in a specific case using the Mithrandir code at the different plateau levels of a quasi-steady T_{CS} scenario (see below); the interpolation of the results was then used to estimate W_{cond} in all cases, at the different temperature levels. W_{cond} increases with the increase of the inlet helium temperature, and at T_{CS} it turns out to be $\leqslant 10\%$ of the Joule power. It should be noted that other authors (Bessette and Mitchell 2008, Kim *et al* 2008, Bruzzone *et al* 2008b, Takahashi *et al* 2008) did not consider W_{cond} in their assessment of V_{cal}, implicitly assuming it to be negligible.

The measured temperatures needed in (2) are assumed to be (1) sufficiently accurate and (2) representative of the whole flow cross section (which would be contradicted in the case of significant transverse temperature gradients). The former issue is addressed here by a procedure which we call, for the sake of simplicity, thermometer 'recalibration': by this we mean the compensation of the offsets measured in dedicated 'baseline' runs (see table 1) where the inlet helium temperature is increased according to a given pattern at $I_{sample} = 0$ kA and B^{ref}_{SULTAN}. The uniform temperature over the cross section requires (at least) plugging the central channel (see table 1), but even in this case temperature gradients can arise in the annular region, as discussed in the next section.

While the mass flow rate is measured only at the outlet, its signal turns out to be approximately constant over a transit time, for the tests considered here. Therefore, we may assume that $\mathrm{d}m/\mathrm{d}t$ is uniform along the conductor (negligible helium compressibility in this phase of the transient), and write

$$\left(\frac{\mathrm{d}U}{\mathrm{d}t}\right)_{CV} = \Phi - W_{cond} - \left(\frac{\mathrm{d}m}{\mathrm{d}t}\right)(h_{out} - h_{in})\,. \qquad (3a)$$

The measurements OF T_{CS} can be performed either with a quasi-steady-state approach (multi-step or staircase heating; see table 1), where the temperature is increased step by step, waiting at each step at least for the transit of the hot helium front through the high-field region, or with a fully transient heating scenario, with the inlet temperature constantly increasing up to the quench of one of the two legs. In both cases, the facility heaters upstream of the helium inlet were used in a balanced way (the same heating applied to the same mass flow rate in both legs, or smaller heating applied to the leg with the lower mass flow rate) in almost all measurements analyzed here, thus avoiding the generation of temperature differences between the two legs.

2.1. Quasi-steady (staircase) heating

In this case, the time derivative of the total internal energy in (3*a*) can be neglected and Φ can be derived from the measured $\mathrm{d}m/\mathrm{d}t$ and temperatures (estimating W_{cond} as discussed above):

$$\Phi = W_{cond} + \left(\frac{\mathrm{d}m}{\mathrm{d}t}\right)(h_{out} - h_{in})\,. \qquad (3b)$$

The recalibration of the thermometer was performed in this case through a dedicated quasi-steady or staircase baseline run, performed in thermal–hydraulic conditions relevant for the respective T_{CS} tests, where the temperature profile along the conductor was measured at increasing inlet temperatures (see figures 4(b)–(d)). The procedure is based on the assumption that all (longitudinal and transverse) temperature gradients measured in the conductor *in the absence of Joule heating* ($I_{sample} = 0$ kA) can be treated as an offset, which is consistent with the adiabatic assumption above[3]. Different temperature readings at different locations could be related, for instance, to the magneto-resistance of the sensors, as suggested in Calvi (2007).

After correcting the temperatures at zero external heating ($T_{in} \sim 4.5$ K), the results of the baseline run for all samples tested with quasi-steady heating are summarized in figure 5 (the TFPRO2 re-test is discussed in a dedicated section below). The temperature differences T5 − T3 and T6 − T4, are always within ± 0.01 K; this may be compared with the measurement accuracy of ± 2 mK on temperature differences (Bruzzone *et al* 2007), which was well confirmed by the polarity checks performed during the TFPRO2 re-tests (see below). On the contrary, T7 − T3 and T8 − T4 significantly increase in modulus with increasing T_{in}. Furthermore, basically the same drift is obtained for both KOTF and RFTF1, for which the sensors are physically the same (detached from KOTF and reattached on RFTF1), thus confirming the non-physical nature of these differences.

The temperature differences in figure 5 can be fitted by least squares with a second-degree polynomial, and the following fits will be used as corrections of the raw temperature signals for the evaluation of the enthalpies in (3*a*): for JATF2 (subscript J) we find

$$\mathrm{T5}_{corr} = \mathrm{T5} + m_{5J,1} \times (\mathrm{T3} - \mathrm{T3}_0) + m_{5J,2} \times (\mathrm{T3} - \mathrm{T3}_0)^2 \quad (4)$$

$$\mathrm{T6}_{corr} = \mathrm{T6} + m_{6J,1} \times (\mathrm{T4} - \mathrm{T4}_0) + m_{6J,2} \times (\mathrm{T4} - \mathrm{T4}_0)^2 \quad (5)$$

and for KOTF/RFTF1 (subscript KR)

$$\mathrm{T5}_{corr} = \mathrm{T5} + m_{5KR,1} \times (\mathrm{T3} - \mathrm{T3}_0) + m_{5KR,2} \times (\mathrm{T3} - \mathrm{T3}_0)^2 \quad (6)$$

$$\mathrm{T6}_{corr} = \mathrm{T6} + m_{6KR,1} \times (\mathrm{T4} - \mathrm{T4}_0) + m_{6KR,2} \times (\mathrm{T4} - \mathrm{T4}_0)^2 \quad (7)$$

$$\mathrm{T7}_{corr} = \mathrm{T7} + m_{7KR,1} \times (\mathrm{T3} - \mathrm{T3}_0) + m_{7KR,2} \times (\mathrm{T3} - \mathrm{T3}_0)^2 \quad (8)$$

$$\mathrm{T8}_{corr} = \mathrm{T8} + m_{8KR,1} \times (\mathrm{T4} - \mathrm{T4}_0) + m_{8KR,2} \times (\mathrm{T4} - \mathrm{T4}_0)^2 \quad (9)$$

where $\mathrm{T3}_0$ and $\mathrm{T4}_0$ are the values of T3 and T4, respectively, before the inlet heating is turned on, and the coefficients of the fits are reported in table 2.

In the calibration runs, the computed V_{cal} after the signal correction is on average 0, as shown in figures 6(b)–(d), confirming the adopted procedure.

[3] The whole recalibration procedure could be equivalently justified even if the conductor was not adiabatic, provided the heat sources/sinks were constant and in particular unaffected by the transport current and temperature increase: if the temperature differences are small enough, which is always verified in our case, these sources/sinks are canceled out by the recalibration of the sensor. The independence of heat sources/sinks on the temperature increase is verified *a posteriori* by the fact that the same recalibration fits hold in the whole temperature range of the baseline runs, thus confirming the absence of other temperature-dependent effects.

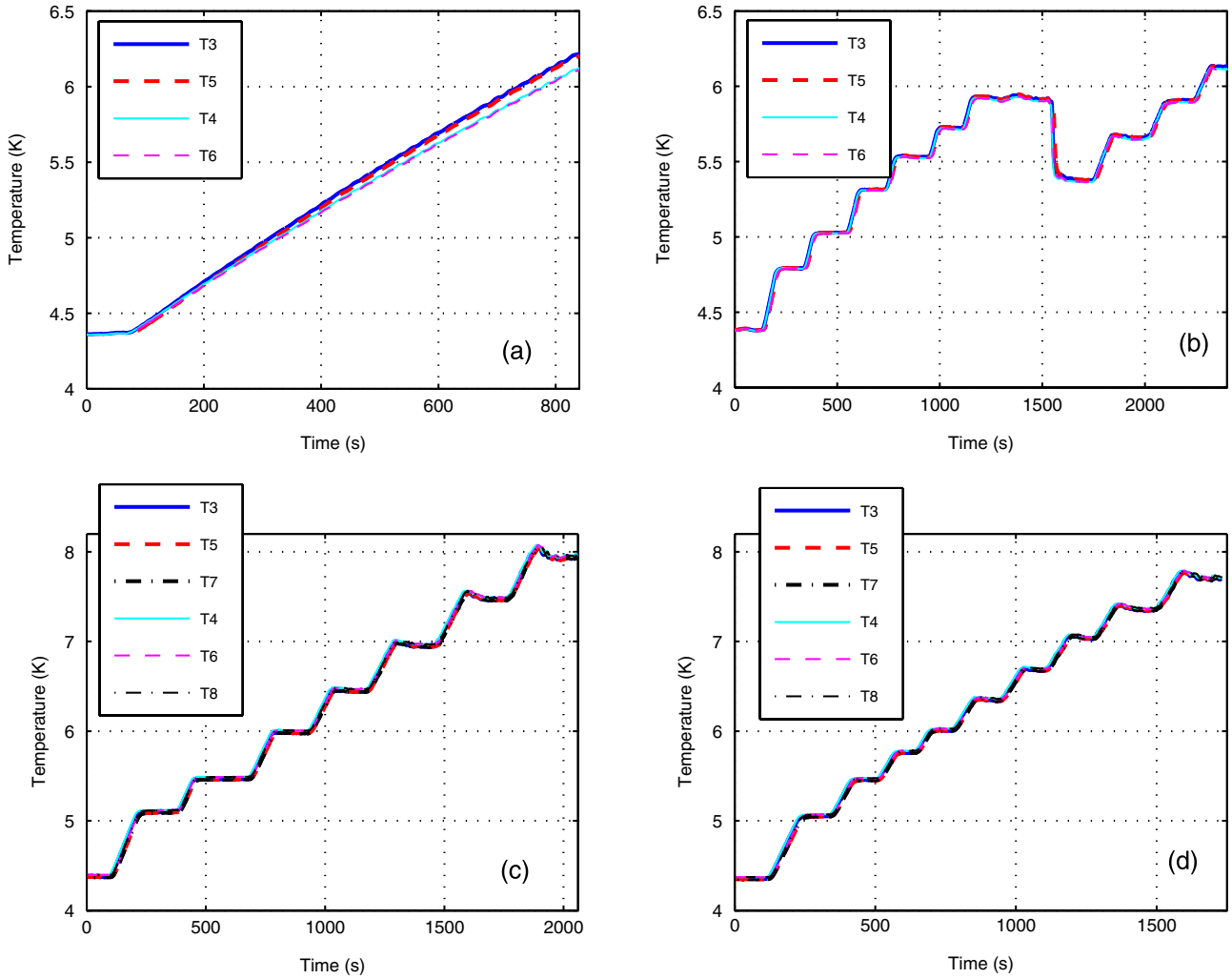

Figure 4. Evolution of the temperature (recalibrated signals) at the different sensor locations in the baseline runs (no transport current, reference background magnetic field) for the different samples: (a) TFPRO2 (transient), (b) JATF2, (c) KOTF and (d) RFTF1. A moving average on 50 points has been applied to the raw T signals.

Table 2. Coefficients of temperature calibration fits (4)–(9) for the samples JATF2, KOTF and RFTF1.

	$m_{5x,1}$	$m_{6x,1}$	$m_{7x,1}$	$m_{8x,1}$	$m_{5x,2}$	$m_{6x,2}$	$m_{7x,2}$	$m_{8x,2}$
J	0.0002	−0.0022	NA	NA	0.001	−0.0009	NA	NA
KR	0.0037	0.0035	0.0232	0.0192	−0.0018	−0.0008	−0.0026	−0.0022

2.2. *Transient heating*

In this case, $\mathrm{d}U/\mathrm{d}t$ in (3*a*) cannot be neglected. Indeed, for the phases of the transient when Φ (and therefore W_{cond}) is negligible we get from (3*a*):

$$\left(\frac{\mathrm{d}U}{\mathrm{d}t}\right)_{\mathrm{CV}} \approx \left(\frac{\mathrm{d}m}{\mathrm{d}t}\right)(h_{\mathrm{in}} - h_{\mathrm{out}}) \approx \left(\frac{\mathrm{d}m}{\mathrm{d}t}\right) \times (h_{\mathrm{in}}(t) - h_{\mathrm{in}}(t - \Delta t)). \quad (10)$$

The second approximation in (10) assumes the pure advection of the temperature along the conductor, where Δt is the transport time between the two thermometers.

We now further assume that $\mathrm{d}U/\mathrm{d}t$ does not vary significantly when Φ (and W_{cond}) is $\neq 0$, i.e. that Joule heating (and conduction) contributes only to the enthalpy variation across the CV. Then we can use (10) as a rough estimate of $\mathrm{d}U/\mathrm{d}t$ for the whole transient and substitute into (3*a*) to obtain

$$\Phi \approx W_{\mathrm{cond}} + \left(\frac{\mathrm{d}m}{\mathrm{d}t}\right)(h_{\mathrm{out}}(t) - h_{\mathrm{in}}(t - \Delta t)). \quad (11)$$

The error introduced by the assumptions leading to (11) from (3*a*) was estimated as ∼0.1 K on T_{CS} by means of a Mithrandir simulation of a transient T_{CS} measurement with comparable $\mathrm{d}T_{\mathrm{in}}/\mathrm{d}t$ as in the tests; the simulation results were then post-processed comparing the T_{CS} computed by evaluation of the average voltage across the high-field region and by calorimetry.

Also in the transient case a thermometer recalibration is needed, and it can be performed using a transient baseline run, where the temperature gradients T5 − T3 and T6 − T4 are

monitored for continuously increasing inlet temperatures, at $I_{\text{sample}} = 0$ kA and $B^{\text{ref}}_{\text{SULTAN}}$.

Among the samples for which a transient strategy had been applied for the T_{CS} measurements, a dedicated (transient) baseline run was performed only in TFPRO2 (see figure 4(a)). The correction to be applied to T5, T6 has been computed in this case imposing Φ, $W_{\text{cond}} = 0$ in (11). We get:

$$\text{T6}_{\text{corr}} = \text{T6} + m_6 \times (\text{T4} - \text{T4}_0) \qquad (12)$$

with $m_6 = 0.0055$, whereas no correction is needed for T5. This correction was validated in the first part of a T_{CS} measurement at 40 kA ($T < 6.5$ K), where $\Phi = 0$ on average was obtained (not shown), as expected.

No recalibration was possible on TFPRO1, since no dedicated baseline run was performed; the calorimetric analysis in that case therefore suffers from large uncertainties (Savoldi Richard and Zanino 2007).

3. Evaluation of uncertainties in the calorimetric estimation of T_{CS}

The recalibration procedure described above allows the reproduction of a zero voltage with zero transport current (see figure 6), with an accuracy on average better than ± 0.5 μV. We will then consider this accuracy on the voltage as an indication of the typical error in the calorimetric assessment of T_{CS}. The effect of this error on the T_{CS} error bar depends, however, on the conductor n-index, a lower n-index giving broader uncertainty on T_{CS} (see below).

Two other issues affect the calorimetry and are addressed below[4]. They are related to possible inhomogeneities on the conductor cross section of either: (A) the temperature (related to non-uniform heat generation inside the cable bundle region or at the joint, for example), or (B) the mass flow rate (related to the opening of a 'third channel' or gap in the cable bundle space due to the cable displacement driven by Lorentz forces in the high-field region, for example). These two items have been investigated using the M^3 code (Savoldi Richard *et al* 2007), which allows an arbitrarily refined discretization in the CICC cross section with respect to the limited number of cable components included in the Mithrandir model.

3.1. Impact of temperature inhomogeneity on the cross section

When we reach T_{CS} during the SULTAN tests, a temperature increase $\Delta T_{\text{crit}} \sim 20$ mK across the high-field region is expected for a mass flow rate of, say, 3 g s^{-1}, due to Joule heating $E_{\text{C}} \times \Delta L \times I_{\text{sample}}$. Therefore, as a rule of thumb, a maximum temperature inhomogeneity of, say, $\Delta T_{\text{crit}}/10$ (i.e. lower than a few mK) is required on the conductor cross section and along the conductor, far from T_{CS}, in order to apply (2) with acceptable accuracy. Transverse gradients

[4] The effect of the self-field on the temperature sensors has not been considered here, since the temperature sensors are located on the magnetic load neutral line, i.e. on the plane parallel to the direction of B_{SULTAN} and passing through the conductor axis, where the magnetic self-field amplitude is only a few per cent of the total magnetic field (~0.5 T over ~11 T at 68 kA), giving a second-order correction to the recalibration curves.

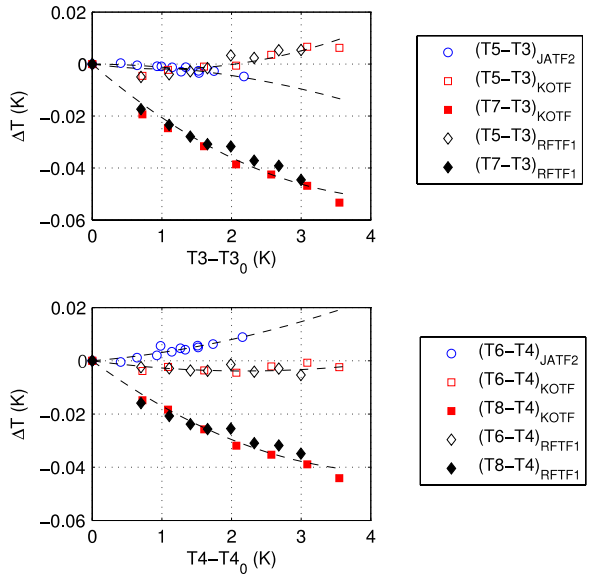

Figure 5. Temperature difference between different sensors across the high-field region at $I_{\text{sample}} = 0$ kA, $B^{\text{ref}}_{\text{SULTAN}}$, for the left leg (a) and right leg (b), respectively. Parabolic fits are also shown (dashed lines) applied separately to JATF2 and to KOTF/RFTF1.

would imply the need for different thermometers on the same cross section to accurately assess the average inlet and outlet enthalpies. Longitudinal gradients have to be excluded in the absence of Joule heating, unless they result from the downstream propagation of upstream transverse gradients, combined with the mismatch between pitch length of the petals and distance between the thermometers.

As already mentioned above, when testing KOTF and RFTF1 it was possible to check the temperature homogeneity on the conductor cross section, thanks to the presence of two opposite sensors downstream of the high-field region. Very good temperature homogeneity was recorded for both samples in the left legs. On the contrary, a temperature difference $\geqslant$20 mK was measured for both right legs, already at the end of the current ramp and still before turning on the inlet heater, both between T6 and T8 and between T6 and T4. The temperature gradient, measured both on a cross section downstream of the high-field region and across the high-field region itself (while, the measured difference between T8 and T4 was one order of magnitude lower), could be due for instance to measurement errors or to non-uniform heating in the joint. However, there is no way to positively assess the reliability of either option. In this condition, the calorimetric analysis can lead to ambiguous results depending on which (combinations of) temperatures are chosen to compute the enthalpy at the CV outlet (see figure 7), which is unacceptable. Therefore, a calorimetric assessment cannot be performed on these two conductors.

3.2. Impact of inhomogeneity of the mass flow rate on the cross section

Since the central channel is blocked in the considered CV, the whole flow is in the petals (the mass flow rate in the so-

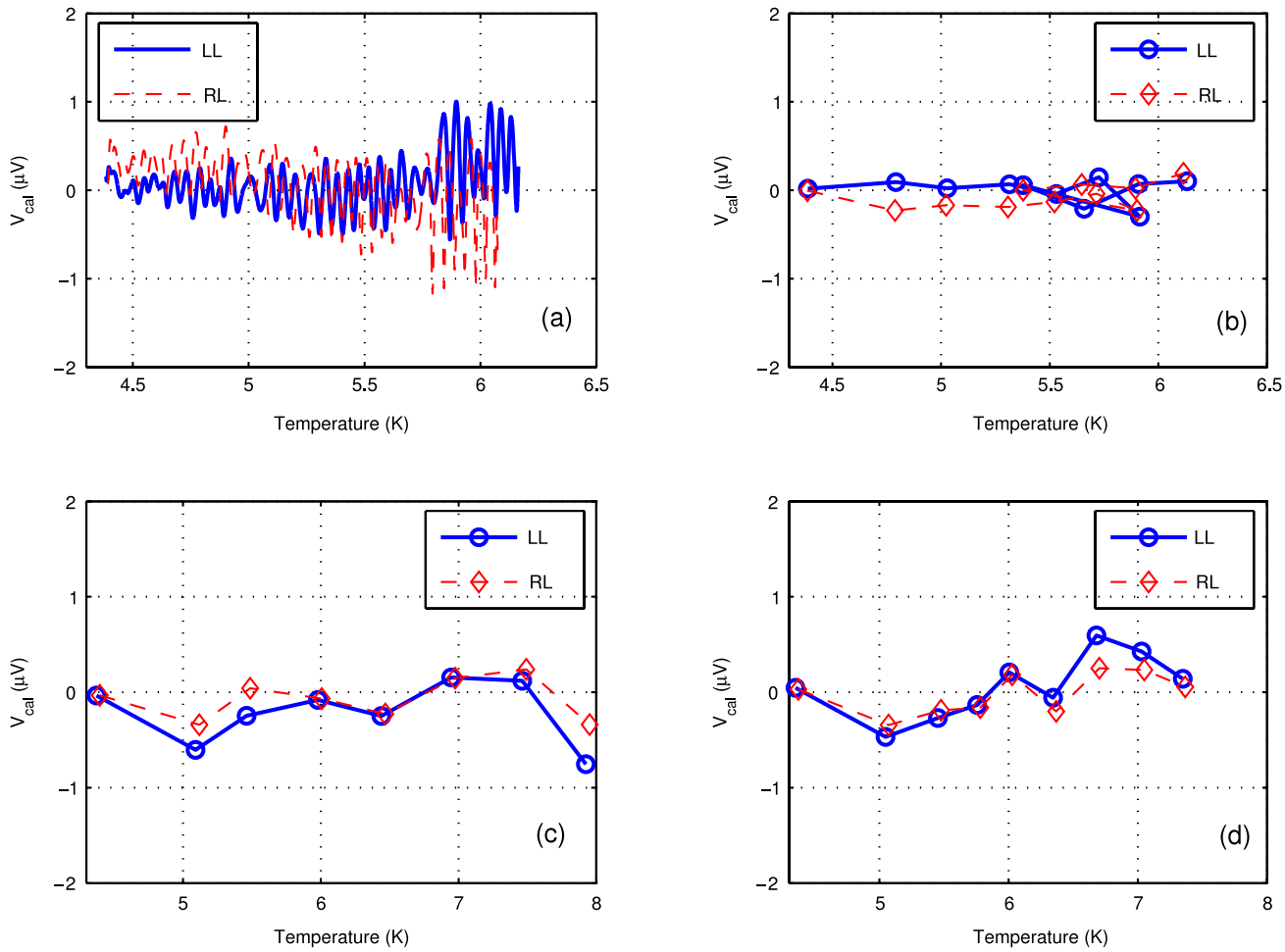

Figure 6. Computed V_{cal} in the baseline runs ($I_{sample} = 0$ kA, $B_{SULTAN} = B^{ref}_{SULTAN}$) for the different samples: (a) TFPRO2 (transient), (b) JATF2, (c) KOTF and (d) RFTF1. Although $I_{sample} = 0$ kA for these runs, we computed V_{cal} here using (1) and $I_{sample} = I^{ref}_{sample}$, in order to translate the error in the estimated power Φ into an estimate relevant for the voltage error assessment under reference T_{CS} test conditions.

called triangles should be negligible here, in view of the high conductor compaction).

If a gap opens on the less loaded side of the conductor (Hamada *et al* 2004), where the magnetic field has its peak, the mass flow rate fraction in the petals decreases because of the reduced flow area. If the cable deforms elliptically, the re-partition of the total (imposed) mass flow rate between the gap and the petals can be computed analytically, relying, for example, on the Katheder correlation for the petal region and on the smooth tube correlation for the gap. The opening of a gap of $<\sim$0.5 mm (which would already be large, in view of the already high conductor compaction) may lead to a reduction of mass flow in the petals $<10\%$ for a total mass flow rate $\sim$3 g s^{-1}. The main effect on calorimetry is that only a (gap-dependent) fraction of the total mass flow rate is Joule heated, assuming that the gap flow channel is approximately adiabatic. The effect on the calorimetric assessment of T_{CS} would be a maximum overestimation of V_{cal} by $\sim$10%, i.e. less than 0.5 μV in the worst case, and the T_{CS} computed neglecting this effect is in any case a conservative estimate.

However, the gap opening would affect the calorimetry only when the sensors located just downstream of the high-field region are used, while during the re-test of TFPRO2 the calorimetric exercise on the right leg shows that the T_{CS} computed using the far-downstream sensors gives essentially the same results as that computed using the sensors closer to the high-field region (see below). This indicates that the error introduced by the opening of a third channel is *de facto* negligible, at least in the TFPRO2 case.

4. Results

The calorimetric approach is applied here systematically to the T_{CS} assessment of the TF samples. Comparison between calorimetric and electrical characteristics is discussed. As for the latter, both raw data and 'corrected' characteristics in the form of the power law $V = V_0(T/T_{CS})^m$ (Bruzzone *et al* 2008b) are considered. For all cases of quasi-steady (staircase) heating, the calorimetric estimate of T_{CS} is determined as the temperature at which the similar power law fit of the V_{cal} data (plateau values) reaches the value V^{thres}_{cal}. In the case of transient heating, the whole calorimetric characteristic is directly computed.

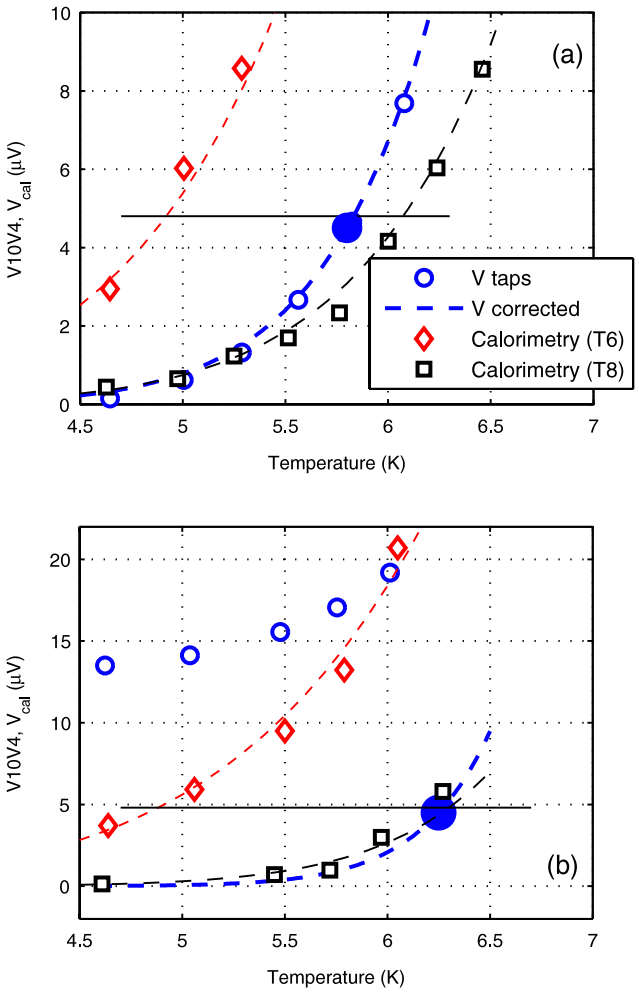

Figure 7. VT characteristic of the T_{CS} test at 1000 cycles for (a) the KOTF sample, right leg and (b) the RFTF1 sample, right leg, respectively, from voltage taps (open circles) and reconstructed from calorimetry using T6 (open diamonds) and T8 (open squares) in the computation of the downstream enthalpy, respectively. The temperature in the abscissa is $T_{ave} = (T6 + T8)/2$ for the electrical characteristic, and T6 and T8, respectively, for the points reconstructed from calorimetry. The voltage corrected according to the recipe in Bruzzone *et al* (2008b) is also reported (thick dashed line), together with the fit of the (steady-state) calorimetry results (thin dashed-dotted line for calorimetry with T6 and thin dashed line for calorimetry with T8, respectively). The horizontal line corresponds to V_{cal}^{thres}. The T_{CS} value obtained by Bruzzone *et al* (2008b) is also reported (solid circle).

The T_{CS} values obtained by the different methods and authors are summarized in table 3 at the end of this section. The comparison between electrical and calorimetric assessments can be used to estimate the uncertainty of the measurement (Bessette and Mitchell 2008).

The tests with the reference instrumentation are considered first. The calorimetric assessment of the TFPRO2 re-test with extended diagnostics is then briefly discussed, confirming the calorimetric analysis performed on the test with standard diagnostics. The JATF2 re-test is not considered here, since on this sample, as we shall see below, there is already a good agreement between our calorimetric assessment and (most of the) other authors, based on standard instrumentation only.

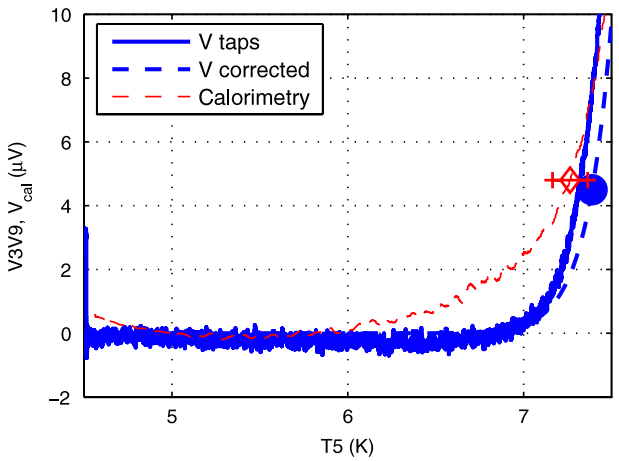

Figure 8. TFPRO2 OSTII (left) leg. VT characteristic of the T_{CS} test at 1000 cycles, from voltage taps without corrections (thick solid line, obtained with a moving average on 50 points on raw V and T signals), from voltage corrected according to the recipe in Bruzzone *et al* (2008b) (thick dashed line) and reconstructed from calorimetry (thin solid line, obtained with a moving average on 50 points on raw T, p, dm/dt signals and an additional moving average on 100 points on the resulting enthalpy differences). The T_{CS} value obtained from calorimetry is indicated (solid diamond), together with its error bar, as well as the T_{CS} value from Bruzzone *et al* (2008b) (solid circle). While the T_{CS} values obtained from calorimetry and from electrical measurements are directly comparable, the electrical and calorimetric characteristics are not directly comparable because they refer to different conductor lengths.

Table 3. Results of the performance assessment of ITER TF short samples tested in 2007 in SULTAN.

		T_{CS}	
Sample	Leg	Calorimetric	Electric
TFPRO2	OSTII	7.27 ± 0.10 7.30[b]	7.33–7.35[a]
	OSTI (1st test)	5.66 ± 0.17 6.00[b]	6.16–6.50[a]
JATF2	JAB2	6.33 ± 0.11 6.40–6.60[b]	5.50–6.40[a]
	JAI2	5.95 ± 0.07 5.8–6.1[b]	5.77–5.95[a]
KOTF	L	5.44 ± 0.08 5.50[b]	5.45–5.50[a]
	R	[c] 5.45[b]	5.65–5.80[a]
RFTF1	L	6.03 ± 0.05	5.90[a]
	R	[c]	6.25[a]

[a]Bruzzone *et al* (2008b) and Bessette and Mitchell (2008) from voltage taps across the high-field region ($V3$ $V9$ or $V10$ $V4$).
[b]Bessette and Mitchell (2008) and Takahashi *et al* (2008).
[c] Calorimetric assessment is unreliable in this case, see text.

4.1. Samples tested with 'standard' instrumentation

The electric results for the TFPRO2 OSTII (left) leg (Bruzzone *et al* 2008a) are confirmed by the (transient) calorimetric approach (see figure 8).

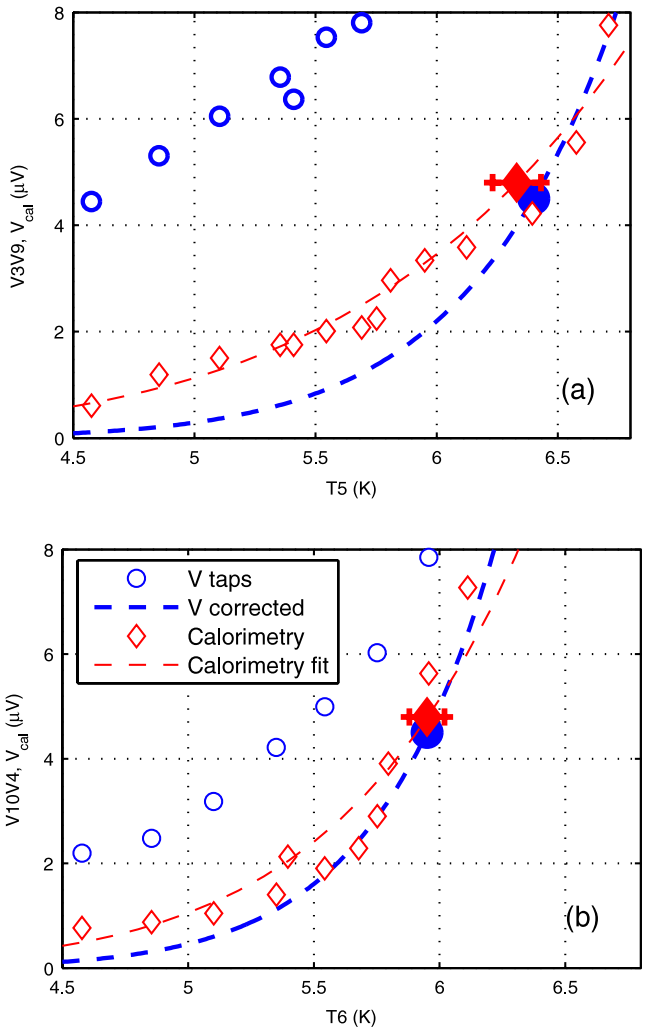

Figure 9. JATF2 sample, VT characteristic of the T_{CS} test at 1000 cycles, from voltage taps without corrections (open circles) and reconstructed from calorimetry (open diamonds), for the JAB2 (left) leg (a) and JAI2 (right) leg (b), respectively. The voltage corrected according to the recipe in Bruzzone *et al* (2008b) is also reported (thick dashed line), together with the fit of the (steady-state) calorimetry results (thin dashed line). The T_{CS} value obtained from calorimetry is indicated (solid diamond), together with its error bar, as well as the T_{CS} value from Bruzzone *et al* (2008b) (solid circle).

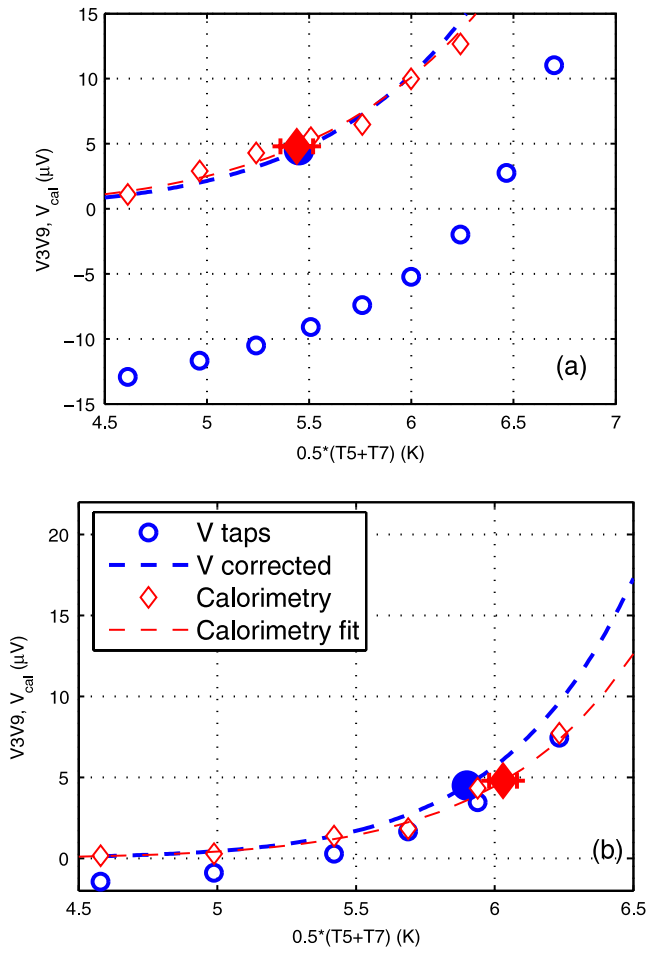

Figure 10. VT characteristic of the T_{CS} test at 1000 cycles for (a) KOTF sample, left leg, and (b) RFTF1 sample, left leg, respectively, from voltage taps without corrections (open circles) and reconstructed from calorimetry (open diamonds). The voltage corrected according to the recipe in Bruzzone *et al* (2008b) is also reported (thick dashed line), together with the fit of the (steady-state) calorimetry results (thin dashed line). The T_{CS} value obtained from calorimetry is indicated (solid diamond), together with its error bar, as well as the T_{CS} value from Bruzzone *et al* (2008b) (solid circle).

The (transient) calorimetry on the TFPRO2 OSTI (right) leg gives, for the T_{CS} measurement at 1000 cycles, a slightly higher value than that computed from the electrical signals without correction. In both cases (measured and calorimetric voltage) the signal at the end of the ramp already shows some current sharing (not shown). Different corrections of the voltage signals, however, give much higher T_{CS} values—compare Bruzzone *et al* (2008b) with Bessette and Mitchell (2008). The T_{CS} value determined here by transient calorimetry is slightly below the calorimetric estimate in Bessette and Mitchell (2008), possibly because the transient contribution (as well as W_{cond}) in equation (3*a*) was neglected by those authors.

For JATF2, the calorimetry on the JAB2 (bronze route, left) leg gives a completely different picture from the raw electric signals (see figure 9(a), where a voltage close to the T_{CS} threshold was measured already at the end of the current ramp), but the resulting T_{CS} is in very good agreement with the estimate from the corrected electrical characteristic (Bruzzone *et al* 2008b), as well as with the calorimetric estimate in Takahashi *et al* (2008). In contrast, the T_{CS} deduced from the voltage signals in Bessette and Mitchell (2008) is almost 1 K below our calorimetric estimate.

In the JATF2 JAI2 (internal tin, right) leg (figure 9(b)), the T_{CS} assessed by calorimetry is again in good agreement with the analysis of Takahashi *et al* (2008), but the error bar is smaller (± 0.07 K) than that in JAB2 in view of the larger n-index of the cable (see above). In both JATF2 legs, the VT characteristic reconstructed from calorimetry foresees a voltage $<0.5\ \mu$V (i.e. zero within the error bar) at the end of the ramp, as a consequence of a temperature difference across the high-field region within $\sim$5 mK. The absence of a significant offset at the end of the ramp supports the fact that T5 and T6 are representative of the average temperature on the conductor cross section, and that no significant Joule heating is present in the high-field region.

In the case of the KOTF sample, left leg, the raw voltage signal showed a very large and negative voltage at the end of the current ramp (see figure 10(a)). The T_{CS} found here is again in good agreement with the corrected electrical assessment from Bruzzone *et al* (2008b) (see figure 10(a)), and also with Bessette and Mitchell (2008) and Kim *et al* (2008).

In the case of the RFTF1 sample, left leg (Shikov *et al* 2008), where only a marginal difference between T5 and T7 (on the same cross section) was present, the calorimetric estimate supports the corrected electrical estimate from Bruzzone *et al* (2008b) (see figure 10(b)).

4.2. TFPRO2 re-test with enhanced instrumentation

In view of the difficulties in the interpretation of the T_{CS} measurements in many tested samples, a new set of diagnostics was implemented on the TFPRO2 sample (whose left leg had shown outstanding performance during the first test), including both additional stars of voltage taps (Bessette 2007) and additional pairs of thermometers, located along the conductor as shown in figure 2(b) and mounted on the jacket on the two opposite sides of the magnetic load neutral line.

The thermometers just downstream of the high-field region, T6/T6a and T8/T8a for instance, are located at a distance of $\sim 1/6$ of the petal twist pitch length ($\sim$500 mm in this case, according to the measurement performed at CRPP) from each other, so that they can be considered representative of the temperature of about four different petals. The same rationale is behind the choice of the location of the thermometers further downstream on the conductor (e.g. T10/T10a, T12/T12a).

With the aim of clarifying the error bars in the calorimetric assessment of T_{CS}, a careful check of the sensor precision (i.e. the measurement repeatability in the same operating conditions) was performed, varying the polarity of the sensor current. The accuracy of the sensor measurements (i.e. the capability of the temperature sensor to indicate the actual temperature) was assessed by measuring the drift with respect to temperature and magnetic field. Under the assumption that, in the absence of external heat sources, the temperature must be homogeneous in the conductor, the temperature drift can be compensated and the signals can be recalibrated, as already done above for the samples with standard diagnostics, using the data of a baseline run at zero transport current and B^{ref}_{SULTAN}.

Hardly anything can be said about the left leg re-test from the calorimetric point of view. Selected T_{CS} tests were performed unbalancing the mass flow rate in the two legs, with a lower mass flow rate in the stronger left leg, in order to reach higher temperatures there. However, above a temperature level that is still relatively lower than T_{CS}, clear temperature plateaus were not achieved[5].

As a major difference with respect to the first test campaign, the T_{CS} during the re-test was also measured in TFPRO2 using the quasi-steady strategy, so that only the steady-state temperature values should be considered for the calorimetric analysis. The steady state should also guarantee that the readings of the temperature sensors located where the central channel is open (T10–T12) are not affected by radial temperature gradients due to the presence of the central channel. Thus the calorimetric evaluation of the Joule heating in the conductor can be performed here both across the high-field region strictly speaking, as done so far for the samples with standard instrumentation, and across longer sample lengths. In both cases an average of the four signals located at one-sixth of the petal pitch is used to obtain the outlet enthalpy, whereas the average between T4 and sT4a is used to obtain the inlet enthalpy.

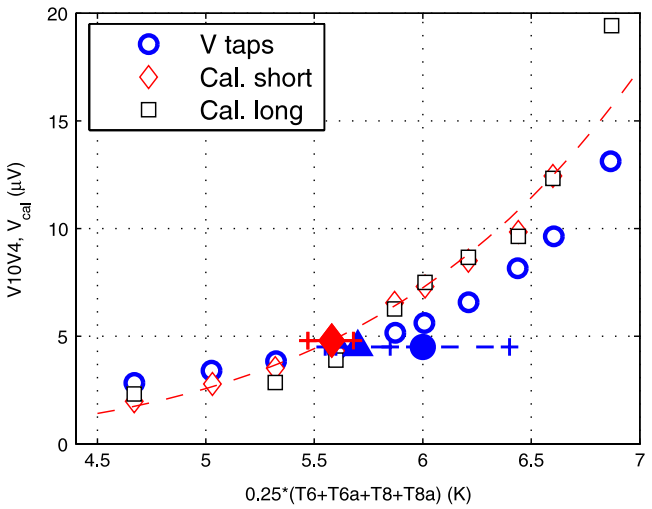

Figure 11. TFPRO2 sample, right leg, first T_{CS} measurement during the re-test campaign: VT characteristic from voltage taps (open circles) and reconstructed from calorimetry at the average temperature between T6, T6a, T8 and T8a (open diamonds) and at the average temperature between T10, T10a, T12 and T12a (open squares). The T_{CS} value obtained from calorimetry is indicated (solid diamond), together with its error bar, as well as the T_{CS} value from Van Lanen and Nijhuis (2007) (solid triangle).

The analysis of the TFPRO2 re-test results is reported in figure 11. First, it can be noted that the agreement between the voltage reconstructed from the two different sets of downstream sensors (T6/6a/8/8a and T10/10a/12/12a) is excellent. This confirms that, as expected, no significant voltage is generated in the sample outside the high-field region. Also, the raw (uncorrected) electrical and calorimetric characteristics are in much better agreement than in most of the cases above. The resulting value of T_{CS} is also in very good agreement with the calorimetric evaluation of T_{CS} in the first campaign, performed using the transient strategy (see above), thus confirming the validity of that approach at least for the present sample. A preliminary evaluation of the results of the enhanced electrical diagnostics also supports this result (Van Lanen and Nijhuis 2007).

5. Conclusions

A new generation of ITER TF conductor samples was tested in the SULTAN facility during 2007.

[5] Other T_{CS} tests were carried out with the use of the annular heater H1 (see figure 2), but they show heat transfer to the right (colder) leg, outside the joint region. This effect is not taken into account in our calorimetric analysis, which assumes the conductor to be adiabatic along its length, but it is also peculiar to this case only, as in all other cases the heating of the two legs is quite symmetric.

A calorimetric approach to the assessment of conductor performance has been described here in order to allow comparison with and support of the standard but sometimes controversial electrical assessment. The Mithrandir and M^3 codes have been used to estimate the error bars resulting from the assumptions underlying the calorimetric analysis. Typically, the accuracy of the T_{CS} estimate turns out to be of the order of ± 0.1 K.

The results of the present paper are summarized in table 3 and it may be recalled that the ITER criteria for TF conductors require a T_{CS} of at least 5.7 K.

The best performing conductor, OSTII of TFPRO2, shows excellent agreement between electrical and calorimetric assessments. The other TFPRO2 (right) leg, OSTI, showed a significant disagreement between calorimetry and electrical assessments in the first tests. However, while the calorimetric assessment was confirmed in the re-test, the electrical assessment of T_{CS} in the re-test shows excellent agreement with the calorimetry.

For the JATF2/JAI2 conductor the calorimetric and electrical assessments are again in very good agreement. For JATF2/JAB2 the calorimetric estimate supports the more optimistic of the electrical interpretations.

For the KOTF left leg, the calorimetric estimate confirms the electrical interpretations. In the case of the KOTF right leg, the presence of temperature non-uniformities on the cross section makes the applicability of calorimetry questionable.

For the RFTF1 left leg the calorimetric and electrical assessments are in borderline agreement. For the RFTF1 right leg a similar comment applies as for the KOTF right leg above.

Acknowledgments

This work was partially financially supported by the EURATOM Communities under the Contract of Association between EURATOM/ENEA and by the Italian Ministry for University and Research (MUR). The views and opinions expressed herein do not necessarily reflect those of the European Commission. We thank Drs D K Oh, I Rodin, C Sborchia and Y Takahashi for granting permission to use the data presented here from Korean, Russian, EU and Japanese samples, respectively. We also thank Dr P Bruzzone for a critical reading of a first version of the manuscript, Dr D K Oh for discussions, the anonymous referees for many comments which led to a significant improvement of the paper and CRPP Villigen for kind hospitality during the tests.

References

Bellina F, Breschi M, Ribani P L, Savoldi Richard L and Zanino R 2008 Parametric analysis of the ITER TF conductor samples in SULTAN with the THELMA code *ASC08 Conf. (Chicago, IL)*

Bessette D 2007 Additional sensors for the Sultan sample instrumentation, private communication

Bessette D and Mitchell N 2008 Review of the results of the ITER toroidal field conductor R&D and qualification *IEEE Trans. Appl. Supercond.* **18** 1097–100

Breschi M, Bellina F and Ribani P L 2008 Electromagnetic analysis and interpretation of the voltage–temperature and voltage–current characteristics of the ITER TF conductor samples *ASC08 Conf. (Chicago, IL)*

Breschi M and Ribani P L 2007 Electromagnetic modeling of the jacket in cable in conduit conductors *IEEE Trans. Appl. Supercond.* **18** 18–28

Bruzzone P *et al* 2007 Test results of two ITER TF conductor short samples using high current density Nb3Sn strands *IEEE Trans. Appl. Supercond.* **17** 1370–3

Bruzzone P *et al* 2008a Test results of two European ITER TF conductor samples in SULTAN *IEEE Trans. Appl. Supercond.* **18** 1088–91

Bruzzone P *et al* 2008b Results of a new generation of ITER TF conductor samples in SULTAN *IEEE Trans. Appl. Supercond.* **18** 459–62

Calvi M 2007 *Sultan Instrumentation Mtg 26-10-2007 CRPP Memo* unpublished

Cau F, Bagnasco M, Bruzzone P, Calvi M and Roth F 2008 Inter-strand resistance in the termination of ITER conductors *IEEE Trans. Appl. Supercond.* **18** 1101–4

Ciazynski D 2007 Review of Nb_3Sn conductors for ITER *Fusion Eng. Des.* **82** 488–97

Ciazynski D, Duchateau J L, Schild T and Fuchs A 2000 Test results and analysis of two European full-size conductor samples for ITER *IEEE Trans. Appl. Supercond.* **10** 1058–61

Hamada K, Takahashi K, Matsui K, Kato T and Okuno K 2004 Effect of electromagnetic force on the pressure drop and coupling loss of a cable-in-conduit conductor *Cryogenics* **44** 45–52

Heller R, Ciazynski D, Duchateau J L, Marchese V, Savoldi Richard L and Zanino R 2003 Evaluation of the current sharing temperature of the ITER toroidal field model coil *IEEE Trans. Appl. Supercond.* **13** 1447–51

ITER 2004 *Design Description Document. Magnet: Section 1: Engineering Description* N 11 DDD 178 04-06-04 R 0.4

Kim H C, Oh D K, Park S-H, Kim K and Bruzzone P 2008 Development and Sultan test results of ITER conductor samples of Korea *IEEE Trans. Appl. Supercond.* **18** 1084–7

Mitchell N 2005 Operating strain effects in Nb3Sn cable-in-conduit conductors *Supercond. Sci. Technol.* **18** S396–404

Nijhuis A and Ilyin Yu 2006 Transverse load optimization in Nb3Sn CICC design; influence of cabling, void fraction and strand stiffness *Supercond. Sci. Technol.* **19** 945–62

Nijhuis A, van den Eijnden N C, Ilyin Yu, van Putten E G, Veening G J T, Wessel W A J, den Ouden A and ten Kate H H J 2005 Impact of spatial periodic bending and cycling on the critical current of a Nb_3Sn strand *Supercond. Sci. Technol.* **18** S273–83

Savoldi L, Zanino R, Marchese V, Martovetsky N, Suesser M, Ulbricht A, Wuechner F and Zahn G 2002 First measurement of the current sharing temperature at 80 kA in the ITER toroidal field model coil (TFMC) *IEEE Trans. Appl. Supercond.* **12** 635–8

Savoldi Richard L, Bagnasco M and Zanino R 2007 Multi-solid multi-channel Mithrandir (M^3) code for thermal–hydraulic modelling of ITER cable-in-conduit superconductor *Fusion Eng. Des.* **82** 1607–13

Savoldi Richard L and Zanino R 2007 TFPRO1 DC data reduction *PoliTo Memo* unpublished

Shikov A *et al* 2008 Development of a new RF produced internal tin ITER TF conductor sample for testing in Sultan *IEEE Trans. Appl. Supercond.* **18** 1076–9

Takahashi Y *et al* 2008 Performance of Japanese Nb3Sn conductors of toroidal field coils for ITER *IEEE Trans. Appl. Supercond.* **18** 471–4

Taylor D M J and Hampshire D P 2005 The scaling law for the strain dependence of the critical current density in Nb3Sn superconducting wires *Supercond. Sci. Technol.* **18** S241–52

Ulbricht A *et al* 2005 The ITER toroidal field model coil project *Fusion Eng. Des.* **73** 189–327

Van Lanen E P A and Nijhuis A 2007 On extended voltage tap instrumentation used in TFPRO2 retest *Report UT/MATEFU-2007-2* unpublished

Zanino R, Ciazynski D, Mitchell N and Savoldi Richard L 2005 Coupled mechanical–electromagnetic–thermal–hydraulic effects in Nb3Sn cable-in-conduit conductors for ITER *Supercond. Sci. Technol.* **18** S376–82

Zanino R, De Palo S and Bottura L 1995 A two-fluid code for the thermohydraulic transient analysis of CICC superconducting magnets *J. Fusion Energy* **14** 25–40

Zanino R, Savoldi Richard L and The TFMC Testing Group 2003 Performance evaluation of the ITER toroidal field model coil phase I. Part 1: current sharing measurement *Cryogenics* **43** 79–90